Pressure-Induced Conductivity in a Neutral Nonplanar Spin-Localized Radical

Pressure-Induced Conductivity in a Neutral Non-Planar Spin-Localized Radical

Manuel Souto,[†] HengBo Cui,[‡] Miriam Peña-Álvarez,[¶] Valentín G. Baonza,[¶] Harald O. Jeschke,[§] Milan Tomic,[§] Roser Valentí,[§] Davide Blasi,[†] Imma Ratera,[†] Concepció Rovira,[†] and Jaume Veciana*[,†]

[†]Institut de Ciència de Materials de Barcelona (ICMAB-CSIC)/CIBER-BBN, Campus Universitari de Bellaterra, 08193 Cerdanyola del Vallès (Barcelona), Spain

[‡]Condensed Molecular Materials Laboratory, RIKEN, Wako-shi, Saitama 351-0198, Japan

[¶]MALTA CONSOLIDER Team, Departamento de Química Física I, Facultad de Ciencias Químicas, Universidad Complutense de Madrid, 28040-Madrid, Madrid, Spain

[§]Institut für Theoretische Physik, Goethe-Universität Frankfurt, Max-von-Laue-Straße 1, 60438 Frankfurt am Main

KEYWORDS. Single-component conductor, neutral radical conductor, PTM radical, TTF, self-assembly, donor-acceptor system.

ABSTRACT: There is a growing interest in the development of single-component molecular conductors based on neutral organic radicals that are mainly formed by delocalized planar radicals, such as phenalenyl or thiazolyl radicals. However, there are no examples of systems based on non-planar and spin-localized C-centered radicals exhibiting electrical conductivity due to their Mott insulator behavior with large Coulomb energy (*U*) repulsion and narrow electronic bandwidth (*W*). Here we present a new type of neutral radical conductor by linking a tetrathiafulvalene (TTF) unit to a neutral polychlorotriphenylmethyl radical (PTM) with the important feature that the TTF unit enhances the overlap between the radical units as a consequence of short intermolecular S···S interactions. This system becomes semiconducting upon the application of high pressure thanks to increased electronic bandwidth and charge reorganization opening the way to develop a new family of neutral radical conductors.

Introduction

In the last decades, there has been a huge development of molecular conducting materials based on two components, one of which is a π-extended organic acceptor or donor molecule. Such a compositional characteristic is motivated by the need to generate charge carriers in the solid material which is achieved either by a charge transfer (CT) between the donor and acceptor components, if both are present, or by a partial doping of such π-extended molecules with an extrinsic redox agent. These systems have an additional prerequisite for exhibiting electrical conductivity, namely an appropriate packing of the doped molecules that permits the overlap between the frontier orbitals of neighboring molecules along one, two, or even three dimensions of the material.[1-3] More recently, single-component molecular conductors have been developed based on planar metal bis-dithiolene complexes which exhibit structural and electronic characteristics that combine the presence of charge carriers and a proper molecular packing.[4,5] The soft nature of all these molecular crystals permits to tune their electronic properties by applying pressure which allows to switch from a semiconductor material to a metal or even a superconductor. [6-7]

In view of the importance of obtaining crystals of single-component molecular conductors, the use of neutral organic radicals as building blocks for molecular conductors has appeared as alternative due to the possibility that the unpaired electrons can serve as charge carriers without the need of a previous doping process.[8] Phenalenyl-based radicals, developed by Haddon,[9–17] and thiazolyl-based radicals, by Oakley,[18-22] are good examples of such materials. The solid state electronic structure of this kind of crystals is best described in terms of the half-filled band (f = 1/2) Mott-Hubbard model, with one electron associated with each radical site. One of the keys to attain conductivity in these single-component radical-based materials and overcome the charge repulsion problem is to maximize the electronic bandwidth *W* (= 4β) and minimize the intra-site Coulomb repulsion energy *U*. When the electronic bandwidth is sufficient to offset charge repulsion (*W* > *U*), conductivity would take place.[20] Synthetic strategies to produce conductive radical-based materials have focused on the use of highly delocalized planar organic systems, which have the benefit of a low value of *U*, and the incorporation of heavy (soft) heteroatoms in these structures, which can lead to an enhanced bandwidth *W*.[21] However, there are no reported examples of single-component molecular conductors based on non-planar and spin-localized carbon-centered organic radicals due to their weak electronic intermolecular interactions leading to narrow electronic bandwidth and their large intra-site electronic repulsion. Finding new ways to overcome this shortage could expand the

possibilities to generate novel single-component molecular conductors.

Organic molecules containing electron donor (D) and electron acceptor (A) units linked by π-conjugated bridging groups are worthy of attention for the investigation of intramolecular electron transfer phenomena and its associated bistability event.[23] Recently, we have reported a D-A dyad based on a tetrathiafulvalene (TTF), an electron π-donor, connected to a polychlorotriphenylmethyl (PTM) radical, a good electron acceptor, which exhibits bistability in solution through the application of external stimuli such as the polarity of the solvent or temperature.[24-26] Indeed, molecules of this D-A dyad coexist in two electronic structures, one neutral and another zwitterionic, due to the intramolecular charge transfer process between the D and A subunits. Therefore, such a kind of radical D-A dyads are promising candidates to show novel physics when moving from solution to solid state if one takes advantage of the intramolecular CT to generate a doping in the subunits. In order to exploit the physical properties in solid state such as conductivity and magnetism of this kind of species, we have recently obtained the radical donor-acceptor dyad **1** (MPTTF-PTM), based on a PTM radical unit linked to a monopyrrolotetrathiafulvalene (MPTTF) unit through a π-conjugated N-phenyl-vinylene bridge (Figure 1) in order to decrease the steric repulsion between the PTM radical units. This system shows a supramolecular architecture with segregated donor and acceptor units where the TTF units are arranged forming herringbone-type 1-D chains in a close packing of the PTM units.[27]

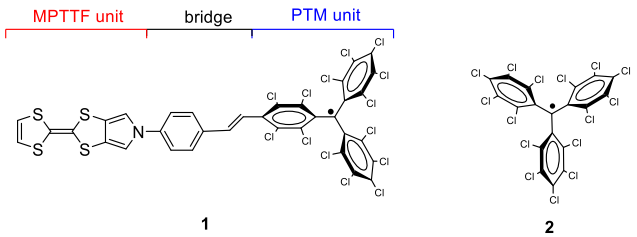

Figure 1. Chemical structures of the neutral radical dyad MPTTF-PTM (**1**) and perchlorotriphenylmethyl radical (**2**).

In this work and in accordance with the intrinsic softness of molecular crystals we report the appearance of conductivity in single crystals of radical dyad **1** induced by pressure in contrast to the Mott insulator behavior of the unsubstituted perchlorotriphenylmethyl radical **2** under all applied pressures. Thus, the conductivity in **1** with pressure is related to the enhancement of the intermolecular overlap between the MPTTF-PTM molecules due to the incorporation of TTF units. This forces the formation of close packed stacks of molecules and, thus, the increase of *W*. Band structure calculations based on density functional theory (DFT) on *ab* initio-predicted MPTTF-PTM crystal structures under pressure confirm the significant increase of *W* in radical dyad **1** as a function of pressure. These calculations suggest important modifications on the electronic structure at pressures above 6-8 GPa with an increase in charge delocalization and of the *W/U* ratio. These effects are clearly observed in our combined analysis of Raman and DFT calculations under pressure. Moreover, high-pressure Raman and photoluminescence spectroscopy show important conformational changes that could indicate a change of the crystalline phase when the system is compressed at high pressures. Up to our knowledge, this is the first example of a single-component molecular conductor based on a non-planar and C-centered neutral radical with highly localized spins that exhibits a semiconductor behavior with high conductivity and low activation energy.

Results

Crystallography. X-ray diffraction analysis on red crystals of radical **2**, obtained by a slow diffusion in a mixture of dichloromethane/hexane (1:1) at room temperature, reveals that it crystallizes in the triclinic system with a space group and the asymmetrical unit is formed by two equivalent molecules (Table S1 and Figure S1 in the Supporting Information). Molecules of **2** are arranged on the *ab* plane as shown in Figure 2 forming regular chains of radicals connected by short Cl···Cl contacts. The distance between the central *ipso*-C (C_1) atoms of two adjacent molecules of PTM radical is 13 Å along the *b*-axis. Moreover, molecules are disposed on the *bc* plane as shown in Figure S2 showing the formation of dimers with a short contact between the phenyl rings (4.3 Å) that are oriented in a parallel position showing a distance between their central *ipso*-carbon (C_1) atoms of 10 Å.

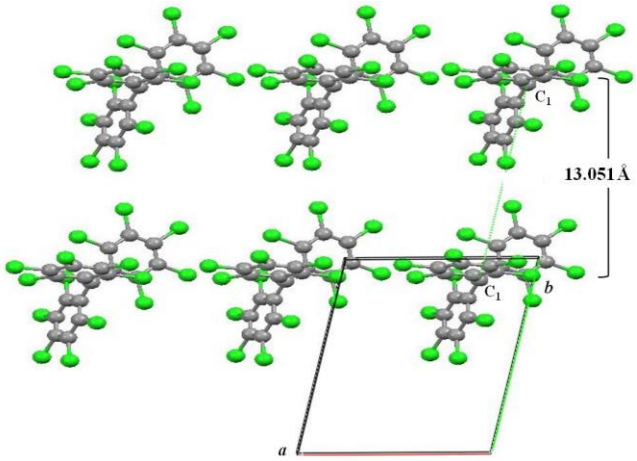

Figure 2. Crystal packing of radical **2** on the *ab* plane. The grey and green ellipsoids represent the carbon and chlorine atoms, respectively. Atoms are shown at the 50% probability level. Intermolecular distance between the central *ipso*-carbons of two adjacent molecules in the *ab* plane (C1···C1') is 13 Å.

On the other hand, dark crystals of radical dyad **1** were also obtained by a slow evaporation in dichloromethane/hexane at room temperature and their X-ray diffraction analysis shows a $P2_1$ space group with Z = 4 (Table S1 and Figure S3).[27] The asymmetric unit shows two inequivalent molecules that are chemically equivalent and exhibit a very similar geometry. Regarding the molecular arrangement, molecules of radical dyad **1** are stacked forming regular 1D chains on the *ab* plane in which MPTTF units are forming a herringbone structure along the *b*-axis with short S···S and Cl···Cl distances of 3.9 and 3.3 Å, respectively (Figure 3). Along this axis direction, the distance between the central *ipso*-carbon (C_1) atoms of the PTM subunit of two adjacent molecules is 7.9 Å and the planes formed by the phenyl rings of the PTM units of adjacent molecules are also oriented in a parallel fashion indicating the formation of π-type interactions between the neighboring radicals units (Figure S4). Thus, the decrease of intermolecular distances between the molecular units clearly denotes a higher packing of PTM radical units in dyad **1** in comparison with radical **2** thanks to the supramolecular self-assembly of the TTF units.

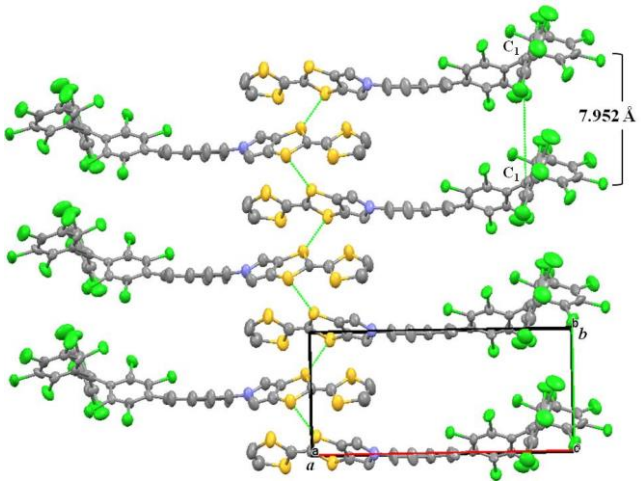

Figure 3. Crystal packing of radical dyad **1** on the *ab* plane showing the intermolecular distance between the central C(1)···C(1)' atoms (7.9 Å) of adjacent PTM molecules and short S···S interactions. The grey, green, blue and yellow ellipsoids represent the carbon, chlorine, nitrogen and sulfur atoms, respectively. Atoms are shown at the 50% probability level. Hydrogen atoms have been omitted for clarity.

High-pressure conductivity. Resistivity measurements on crystals of **1** and **2** were performed under high pressure conditions. Three independent crystals of radical **2** were measured up to 21.2 GPa and they were found always insulating under all assayed conditions. On the other hand, pressure and temperature dependence measurements of the resistivity of radical dyad **1** were also performed with three independent crystals along the *b*-axis (Figures 4, S7 and S8). Crystals of **1** showed insulating behavior at ambient pressure while increasing the pressure the room-temperature resistivity rapidly decreased exhibiting a semiconducting behavior throughout the studied temperature range. From 6.5 GPa the room-temperature resistivity linearly decreased with a negative slope of *ca.* $10^{0.38}$ Ω cm / GPa and the conductivity at 15.2 GPa and 298 K was found to be as high as 0.76 S cm^{-1} with a low activation energy (E_a) of 0.067 eV (E_a = 0.21 eV at P = 6.5 GPa). At higher pressures the room temperature conductivity slightly decreased on increasing the pressure (see Figures S7 and S8) and the conductivity at 21.2 GPa (298 K) was 0.43 S cm^{-1} with and activation energy E_a of 0.073 eV. Reproducibility of measurements was confirmed using three different samples as shown in Figure S8.

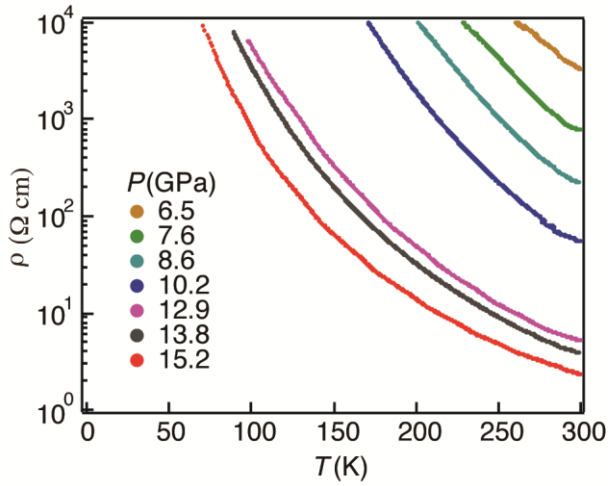

Figure 4. Electrical resistivity of radical dyad **1**. Temperature dependence of the resistivity of radical dyad **1** along the *b*-axis at different pressures.

Magnetic susceptibility. The temperature dependence of the magnetic susceptibility (χ) for a polycrystalline sample at ambient pressure of radical dyad **1** was measured over the temperature range of 2-300 K (Figure S10). The compound shows a Curie-Weiss behavior and the experimental data was fitted to obtain a Curie constant C = 0.394 cm^3 K mol^{-1} with a $\chi_m T$ at room temperature that fully agrees with the theoretical value of 0.375 expected for non-interacting S = ½ systems. Upon cooling, χ_mT decreases according with the presence of weak antiferromagnetic interactions among the radical units (Weiss constant of θ = -1.06 K).

Electrochemical properties. The electrochemistry of radicals **1** and **2** were examined by cyclic voltammetry (Figure S11) in order to have an estimation of the disproportionation potential (E_{disp}). This value can be determined from the potentials $\Delta E_{2\text{-}1} = (E_2^{1/2} - E_1^{1/2})$ of the radical units and provide indirect measurements of the intra-site Coulomb repulsion energy, *U*, which are usually low in highly delocalized spin systems.[17] E_1 electrochemical potential corresponds to the reduction of the radical to the anion and E_2 is attributed to the oxidation process of the radical to the cation. Moreover, in the case of radical dyad **1**, we have the presence of the electroactive TTF unit with two reversible oxidation processes that are located between the reduction and oxidation potentials of the PTM radical that makes more difficult to estimate the disproportionation energy. Indeed, the oxidation of the PTM radical could be affected electrostatically by the presence of TTF^{2+} in close proximity, so we could expect that this value becomes lower for radical **1**. The estimated disproportionation potentials ($\Delta E_{2\text{-}1} = E_2^{1/2} - E_1^{1/2}$) for **1** and **2** are 1.71 and 1.80 V, respectively, confirming that the spin is highly localized in both C-centered radicals.

Table 1. **Electrochemical data of radicals 1 and 2.**

Compound (subunit)	$E^{red}_{1/2}$ (PTM)	$E^{ox1}_{1/2}$ (TTF)	$E^{ox2}_{1/2}$ (TTF)	$E^{ox3}_{1/2}$ (PTM)	E_{disp}[b]
1	-0.19	0.45	0.95	1.52	1.71
2	-0.19	-	-	1.61	1.80

[a]In Volts vs Ag/AgCl; CH_2Cl_2 as solvent and $TBAPF_6$ as electrolyte and scan rate of 0.1 V/s. [b]E_{disp} estimated as $E^{ox3}_{1/2}$-$E^{red}_{1/2}$.

Crystal structures, band structure and charge transfer calculations as a function of pressure. In order to elucidate the microscopic origin of the electrical conductivity pressure dependence in the radical dyad **1** (and in the absence of experimental data for the crystal structures at finite pressures), we relaxed a set of crystal structures at different pressures within density functional theory (DFT) using the projector augmented wave basis as implemented in the Vienna *ab* initio simulation package (VASP)[28-29] and the generalized gradient approximation (GGA)[30] (see Methods section and Supplementary Information for details). The electronic structure and charge transfer of this series of predicted crystal structures was determined with the full potential local orbital (FPLO) basis set.[31] Figure 5 shows the evolution of lattice parameters, monoclinic angle and volume of the predicted structures as a function of pressure. While along the *a* and *b* directions the structures experience a monotonic contraction, this is not the case along the *c* direction (perpendicular to the molecular stacking) where a slight expansion at low pressures

followed by a steep contraction at higher pressures is observed. The decrease of the monoclinic angle indicates a reduction of the structural anisotropy and we observe an enhanced planarity of the molecules at high pressures. Further below we show that our Raman analysis at high pressures is consistent with the predicted structures.

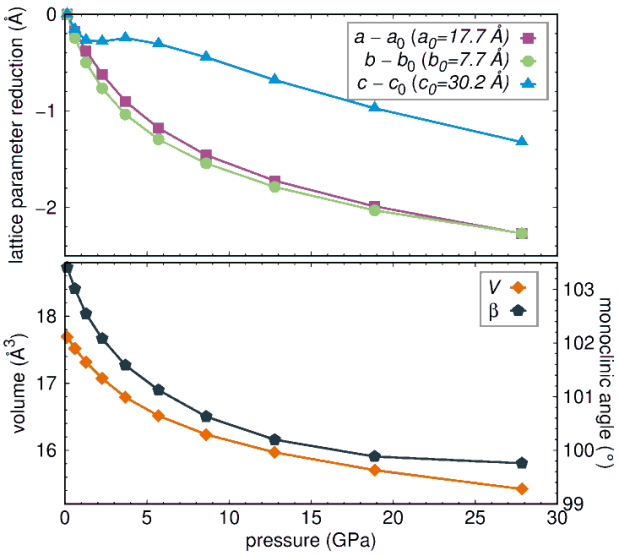

Figure 5. Crystal structure parameters at high pressure. Evolution of lattice parameters, monoclinic angle and volume of the predicted structures of radical dyad **1** as a function of pressure.

We analyze in what follows the electronic structure of radical diad 1 under pressure. Figure 6 shows the GGA electronic bandstructure of the ambient pressure (P=0) structure and the P=8.6 GPa structure. At P=0 the system is a Mott insulator. As it is well known[32] DFT in the GGA approximation is not able to reproduce this insulating state (Figure 6a) due to the insufficient treatment of electronic correlations in GGA. Albeit the absence of a gap at P=0, we can still extract valuable information out of the GGA calculations. There are four half-filled narrow bands at the Fermi level arising from the four molecules per unit cell of **1** (Figure 6a). PTM+bridge is contributing the majority of the carriers in the valence band with some participation of MPTTF. At higher binding energies the bands are mostly of MPTTF character with some hybridization to the PTM+bridge. The lack of dispersion along *kz* indicates that this system is electronically dominantly two-dimensional at ambient pressure. Upon increasing pressure (Figure 6b and S14) the bandwidth *W* significantly increases due to enhanced intermolecular overlap and hybridizations and the system becomes more three dimensional. This increase in *W* and molecular hybridizations contributes to the increase of the ratio *W/U* and the appearance of enhanced conductivity at high pressures as observed in our measurements. At 0 GPa the bandwidth of all four bands at the Fermi level is very narrow (<0.04 eV). However, with pressurization at 8.6 GPa, we observe that the gap in the valence states at -0.05 eV between the bands dominated by TTF orbitals and the bands dominated by PTM orbitals disappears and a wide band manifold of about 0.4 eV forms which is of the same magnitude as the Coulomb barrier estimated from the electrochemical data in solution at ambient pressure. Further compression to 18.9 GPa gives rise to a higher broadening of the bands with bandwidth near 0.8 eV.

Since the susceptibility analysis in the previous section indicated the presence of magnetic interactions among the radical diad units, we have also performed spin-polarized GGA calculations. Figure 8NEW (a) shows the spin distribution in a radical dyad at P=0GPa. We observe a strong spin localization on the central C atom of the PTM units and a less pronounced spin occupation on the MPTTF units. Pressure only slightly influences the spin density distribution between the two components of the molecule. The spin polarized bands show a gap at P=0Gpa (Figure 8NEW (b)) that diminishes and closes at P > 6GPa (Figure 8NEW (c)). Even though we don't have an advanced description of correlations as mentioned above, with the incorporation of magnetism we can track the evolution under pressure of the insulating to semiconducting/metallic behavior associated to magnetism. We observe a closing of the gap between the (spin-polarized) occupied bands with dominant MPTTF character and the empty bands with dominant PTM character. An improved description of correlations -which is beyond the scope of the present study- would shift the closing of the gap to higher pressures as observed experimentally.

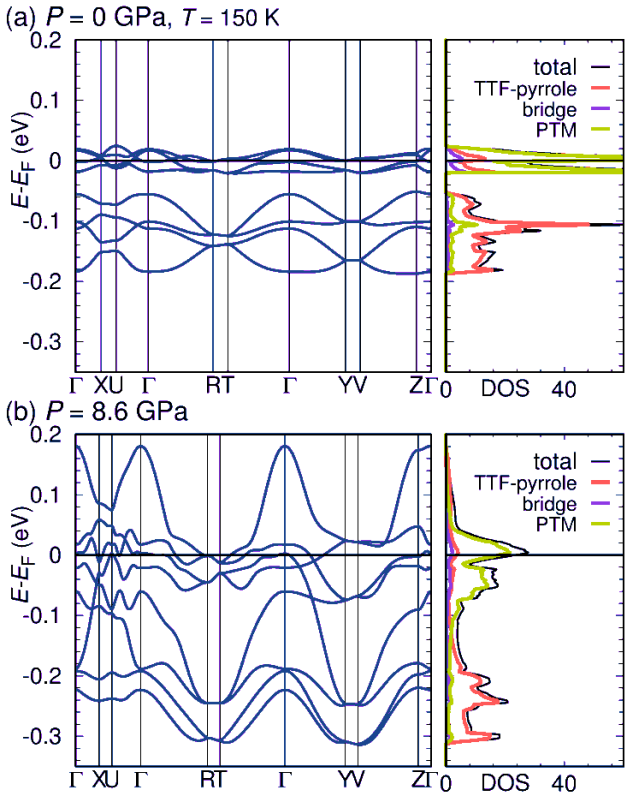

Figure 6. Electronic band structures and density of states of radical dyad **1.** The two-dimensional energy dispersion near the Fermi level at (a) ambient pressure (P=0) and (b) P=8.6 GPa.

Figure 7. Spin-polarized electronic band structures and density of states of radical dyad 1.

The pressure evolution of the charge transfer in the radical dyad 1 is displayed in Figure 8. We chose to distinguish the PTM together with the ethylbenzene bridge as acceptor unit

and the MPTTF as donor unit (Figure 8a). We observe (Figure 8b) that increasing the pressure, the charge transfer between the two units increases from 0.09*e*- at ambient pressure to 0.32*e*- at P = 18 GPa. In In order to analyze the pressure dependence of the charge distribution in the PTM+bridge complex, we plot in Figure 8c the excess charge on PTM and bridge units. We find that increasing the pressure, the PTM unit decreases in excess of charge indicating a possible electron delocalization through the bridge that is in agreement with the enhanced planarity of the system observed in the simulated crystal structures at high pressures. The charge on the donor MPTTF unit increases from 0.09*e*- at ambient pressure to 0.25*e*- at P = 10 Gpa (Figure 8b). Meanwhile, the bridge which is only donating 0.03*e*- at ambient pressure turns into an acceptor with 0.32*e*- extra electrons at P = 10 GPa. This indicates that there is a charge reorganization happening at P = 6-8 GPa between PTM and the bridge. Figure 8c shows the excess charge evolution under pressure for the two inequivalent molecules in the unit cell. These latter results indicate a slight tendency towards molecular charge order in the crystal.

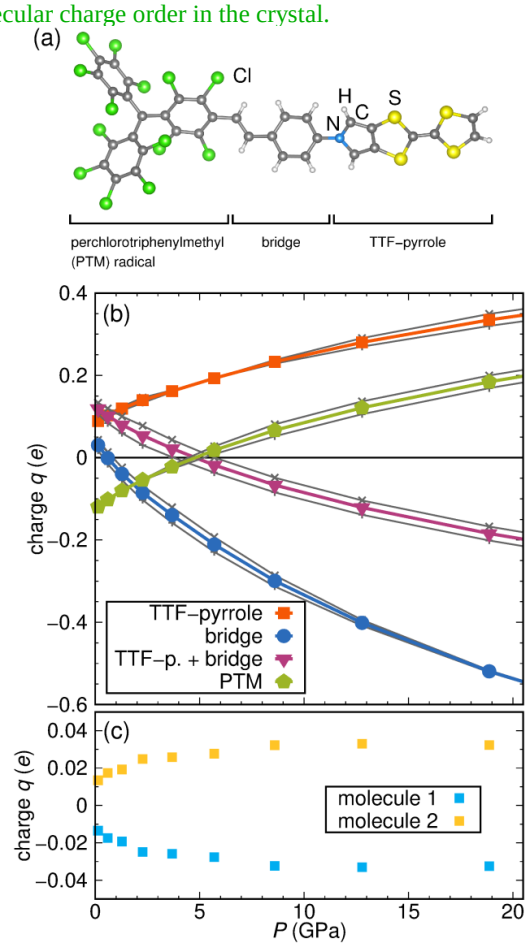

Figure 8. Calculated evolution of excess charge within the units of radical dyad **1** with hydrostatic pressure. (a) The different selected parts of the radical dyad **1**. (b) Excess of charge on the different units under high pressure. (c) Excess of charge on the two non-equivalent molecules of **1** under pressure.

In order to further verify that the here predicted crystal structures provide a realistic account of the radical dyad **1** under pressure, we compare high pressure Raman spectroscopy with spectra obtained from density functional theory calculations on these structures.

High-pressure Raman spectroscopy. The Raman spectra of radical dyad **1** at different pressures were obtained using an excitation wavelength of 532 nm. This study has been complemented by calculation of the spectrum at different pressures based on the density functional theory (DFT) using a Gaussian basis set at the UM06/6-31G(d,p) level.[33,34] The spectra have been calculated for a single molecule whose structure has been extracted from the VASP optimized crystal structures at various pressures in the previous section. This facilitates the Raman analysis by a detailed computational study on the assignment of the bands (See Figures S17-S19). In the 1700-1450 cm^{-1} region, the bands at 1619 and 1597 cm^{-1} are attributed to the C=C stretching modes of the benzene and vinylene units of the bridge whereas the bands in the 1515-1480 cm^{-1} region are mainly due to the C=C stretching of TTF and PTM moieties. The Raman spectra at selected pressures were recorded and their intensity was normalized with the band at 1515 cm^{-1} (C=C stretching of TTF) (Figure S20a). On increasing the pressure, we observed that the Raman bands related to the bridge around 1600 cm^{-1} progressively decreased in intensity. On the contrary, the bands assigned to the TTF and PTM units increased in intensity and overlapped when a high-pressure was applied (Figure S20a). This tendency was also observed for the simulated Raman spectra obtained for the VASP predicted crystal structures at each applied pressure, confirming herewith the same behavior (Figure S20b). Moreover, the overlapping of the bands related to the TTF and PTM units suggests a change of the electronic delocalization on the molecule that could be related to the enhanced planarity of the molecules observed in the simulated crystal structures at high-pressures. On the other hand, in the region around 800 cm^{-1}, the bands attributed to the *out-of-plane* C-H bending broadened and decreased in intensity when increasing the pressure due to the fact that these vibrations were hindered because of the molecular packing.

We have performed a detailed analysis of the relative intensity variation of the measured Raman bands attributed to the vinylene bridge and those related to the PTM and TTF moieties along the entire pressure range to analyze possible phase transitions (Figure 8). We refer to the intensities as the areas of Raman bands, calculating the sum of the areas of the bands at 1619 and 1597 cm^{-1} for the vinylene bridge, the bands at 1570 and 1515 cm^{-1} for the TTF and the bands at 1500 and 1486 cm^{-1} for the PTM unit. We have calculated and plotted the intensity ratio for (*a*) the TTF stretching bands/vinylene bands, (*b*) the PTM stretching bands/vinylene bands, and (*c*) TTF+PTM bands/vinylene bands. A linear fit of the data shows two regions at pressures below and above 8 GPa with different slopes, being the slope steeper at P > 8 GPa. These results suggest that while the system is reorganizing and readjusting the intermolecular spaces up to pressures of 8 GPa, the abrupt change of slope at 8 GPa indicates the presence of important intra- and intermolecular conformational changes that may originate from a crystalline phase transition. Moreover, the evolution of these Raman bands is different from other PTM derivatives previously studied in our group[35] indicating a different electronic behavior for this system.

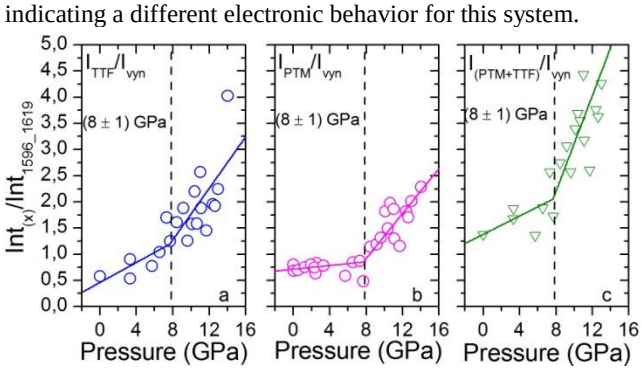

Figure 9. Intensity ratio of Raman bands of radical dyad **1** assigned to (a) C=C stretching of TTF/vinylene, (b) C=C stretching of PTM/vinylene bridge, and (c) C=C stretching of TTF+PTM/vinylene.

Apart from the changes in the relative intensities of the Raman bands, the most apparent effects of pressure on the Raman spectra are the upshifts of the spectral features with increasing pressure. This effect is analyzed in Figure S21 and Figure S22, where the frequencies of the most intense bands of PTM, vinylene bridge and TTF•PTM are plotted as a function of pressure. The observed shifts with pressure show a three regime stage where the different Raman bands shift with different slope with increasing pressure. The three regimes would range from 0 to 2-5 GPa, from 2.5 to 8 GPa and, from 8 to 14 GPa (which is the highest pressure experimentally reached). The first regime is assigned to intermolecular rearrangements, since pressure barely induces any shifting of the bands. In the second one the bands show an important upshift with increasing pressure, indicating that pressure affects bonds and angles, which can be explained by conformational changes to readjust the electronic density. In the third regime, in general all analyzed bands show less steep slopes than in the intermediate regime but steeper than in the first regime. This indicates that pressured larger than 8 GPa must cause both intra- and intermolecular effects. These inter- and intramolecular pressure effects are confirmed by the reversibility observed in high pressure Raman experiments (Figure S23). Up to 1.6 GPa these changes are fully reversible whereas from 6 GPa there are slight deviations between the relative intensities even though the spectral pattern remains. Finally, the recovered sample after compression of about 14.5 GPa is totally different from the pristine one.

High-pressure photoluminescence measurements. In order to further investigate the intra- and intermolecular pressure effect observed by Raman spectroscopy, photoluminescence measurements of crystals of radical dyad **1** when the sample was monochromatically excited with λ = 532 nm at different pressures were performed (Figure 9). High pressure experiments were conducted in a sapphire anvil cell and spectra were recorded at selected pressures up to 12 GPa. Whereas the pristine sample at 0 GPa does not show well defined bands in the visible region, by increasing the pressure it is possible to observe the growth of a broad band in the 600-700 nm region (see Fig. 9 and S24). This band that appears centered at 680 nm (1.8 eV) is much more intense when increasing the pressure above 7 GPa as shown in Figure 9. The photophysical processes observed can be explained by the excitation of dyad **1** with light λ = 532 nm that induces 264α→266α (SOMO→LUMO) electronic transition (See Supporting Information) as it has been already observed in similar systems.[36] At ambient pressure this electronic transition is practically forbidden whereas by increasing the pressure the transition becomes more favored probably due to the enhanced electron delocalization and planarity of the system. Moreover, by increasing the pressure the intermolecular interactions become more important that could lead to an enhancement of the photoluminescence as it has been recently reported.[37,38] In order to analyze the reversibility of the photoluminescence properties at high pressure, we have measured the photoluminescence spectrum of the recovered sample at 6 and 12 GPa (Figure S26). In both cases the intensity of the band remains the same indicating that conformational changes are not reversible and could be originated from a crystalline transition phase.

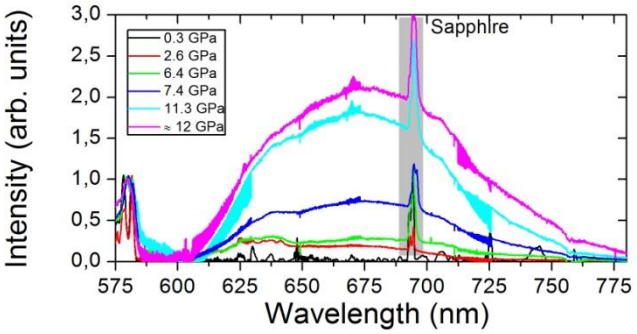

Figure 9. High resolution phtoluminescence spectra of crystals of radical dyad **1** at selected pressures when the sample was excited at 532 nm. The sample was supported on a non-drilled gold gasket and compressed using sapphire anvils with a 380 μm culet.

Discussion

Analyzing all the experimental and theoretical studies, we can assume that the conductivity in radical dyad **1** between neighboring molecules takes place through the enhanced overlap between MPTTF and PTM under pressure. This overlap is absent in radical 2 which remains insulator at all pressures considered. When increasing the pressure, the electronic bandwidth *W* in radical dyad **1** increases until is able to offset the Coulomb repulsion *U*. In addition, there is a remarkable increase of charge transfer between donor MPTTF and acceptor PTM+bridge under pressure. In fact, spin-polarized band structure calculations above 6 GPa show that the gap between the bands dominated by MPTTF orbitals and the bands dominated by PTM orbitals disappear forming a wide band. Moreover, calculations of the evolution of charge transfer indicate that charge reorganization is taking place above the same applied pressures. On the other hand, high-pressure Raman spectroscopy supports this charge reorganization in a similar pressure regime and identical behavior was observed in the simulated spectra obtained for the VASP predicted crystal structures at each applied pressure. Reversibility studies on pressure-dependent Raman and photoluminescence measurements indicate that there is a change in the electronic conformation of the system in agreement with the enhanced planarity of the molecules and the intermolecular reorganization that could hint to a possible structural phase transition.

Summary and conclusions

In summary, we have reported the observation of induced-pressure conductivity in the non-planar and spin localized neutral radical dyad **1** that exhibits a semiconductor behavior with high conductivity and low activation energy upon application of high pressure. In contrast, the model radical **2** remains as a Mott insulator under all applied pressures. This different behavior is due to the supramolecular strategy we have used in order to increase the ratio *W*/*U*. Moreover, the reduction of the effective Coulomb interaction in **1** in comparison to **2** could be attributed to the enhanced electron delocalization in the system due to incorporation of a substituent unit, as confirmed by Raman experiments and theoretical calculations. Overall we believe that the results described here are a proof of concept of a novel strategy providing an important insight into the design of new radical-based conductors. Thus, it may be possible to engineer radicals which can be conducting even without the need for applied pressure.

Experimental section

Synthesis and characterization of radicals 1 and 2. The reagents and solvents used for synthesis and crystallization were of high purity grade (Sigma- Aldrich and SDS SA). Compounds **1** and compound **2** were prepared as previously reported in ref. 27 and 39, respectively. The electrochemical experiments were performed with a potentiostat- galvanostast 263a (EG&G Princeton Applied Research) using platinum wires as counterelectrode and working electrode, a silver wire as reference electrode and as electrolyte a 0.1 M solution of tetrabutylammonium hexafluorophosphate (TBAHFP) in acetonitrile.

Conductivity measurements. The four-probe resistivity measurements were performed with a Cryocooler helium compressor system (Sumitomo Heavy Industries, Ltd.). The KEITHLEY 224 Programmable current source and 182 Sensitive digital voltmeter were used for all measurements.

Raman and photoluminescence measurements. High pressure experiments were conducted in a sapphire anvil cell (SAC)[40,41] with a diameter culet of 360 μm and a gold gasket, specified in each section. No pressure transmitting medium was used and diamond chips were placed as the pressure calibrant. Raman and photoluminescence measurements were performed using an air-cooled argon ion laser, a Spectra-Physics solid state laser, operating at 532.0, nm. The device is equipped with a 10x Mitutoyo long working distance objective coupled to a 10x Navitar zoom system and focused onto the slit of an ISA HR460 monochromator with a grating of 600 grooves mm^{-1} and a liquid nitrogen cooled CCD detector (ISA CCD3000, 1024−256 pixels). Spectra were measured with a spectral resolution of about 2−3 cm^{-1} and calibrated with a standard neon emission lamp. The SAC is mounted on a xyz stage, which allows us to move the sample with an accuracy of 1 μm. The typical sampling area was about 1−2 μm in diameter. The simulated Raman spectra were calculated using the UM06 density functional theory [33] in conjunction with the 6-31G** basis set.[34]

Theoretical calculations. Crystal structures at different pressures were simulated within density functional theory calculations[30] by performing relaxations of lattice parameters, monoclinic angle and internal atom positions at constant volume with the VASP code.[28-29] A plane wave cutoff of 400 eV was used as well as a 4x4x2 k-mesh in the Brillouin zone. We checked, by performing enthalpy calculations that constant volume relaxations were of higher quality than constant pressure relaxations (not shown). All presented bulk electronic structure calculations were performed with the FPLO code[31] where a k-mesh of 6x6x6 points was considered to converge the computations.

ASSOCIATED CONTENT

Supporting Information. Experimental details of X-ray crystallographic data and structure refinement. Supplemental spectra of high-pressure conductivity, magnetic susceptibility, cyclic voltammetry, Raman and photoluminescence experiments of **1**. Simulated Raman spectra and details of theoretical calculations. This material is available free of charge via the Internet at http://pubs.acs.org.

AUTHOR INFORMATION

Corresponding Author

* E-mail: vecianaj@icmab.es

Notes

The authors declare no competing financial interests.

ACKNOWLEDGMENT

This work was supported by the EU ITN iSwitch 642196 DGI grant (BeWell; CTQ2013-40480-R), the Networking Research Center on Bioengineering, Biomaterials, and Nanomedicine (CIBER-BBN), and the Generalitat de Catalunya (grant 2014-SGR-17). This work has also been supported by MINECO through the projects CSD2007-00045, CTQ2012- 38599-C02-02 and CTQ2013-48252-P. M. S. is grateful to Spanish Ministerio de Educación, Cultura y Deporte for a FPU grant and he is enrolled in the Material Science Ph.D. program of UAB. MPA is grateful to the Spanish Ministerio de Educación, Cultura y Deporte for an FPU grant. HO Jeschke, M. Tomic and R. Valenti thank the Deutsche Forschungsgemeinschaft (DFG) for funding through grant SFB/TRR49 and Steve Winter for useful discussions. We thank Carlos Gómez-García (Univ. Valencia) for SQUID measurements as well as Xavier Fontrodona (Univ. Girona) for X-ray diffraction measurements and Mercedes Taravillo (UCM) for the support provided during the high pressure Raman measurements.

ABBREVIATIONS

IET, intramolecular electron transfer; D, electron donor; A, electron acceptor; PTM, perchlorotriphenylmethyl radical; TTF, tetrathiafulvalene.

REFERENCES

(1) Rovira, C. *Chem. Rev*. **2004**, *104*, 5289.

(2) Farges, J. P. *Organic Conductors: Fundamentals and Applications*. Marcel Dekker, New York, USA **1994**.

(3) Bndikov, M.; Wudl, F.; Perepichka, D. F. *Chem. Rev*. **2004**, *104*, 4891.

(4) Nunes, J. P. M.; Figueira, M. J.; Belo, D.; Santos, I. C.; Ribeiro, B.; Lopes, E. B.; Henriques, R. T.; Vidal-Gancedo, J.; Veciana, J.; Rovira, C.; Almeida, M. *Chem. Eur. J*. **2007**, *13*, 9841.

(5) Tanaka, H.; Okano, Y.; Kobayashi, H.; Suzuki, W.; Kobayashi, A. *Science* **2001**, *291*, 285.

(6) Cui, H.; Kobyashi, H.; Ishibashi, S.; Sasa, M.; Iwase, F.; Kato, R.; Kobayashi, A. *J. Am. Chem. Soc*. **2014**, *136*, 7619.

(7) Jerome, D.; Mazaud, A.; Ribault, M.; Bechgaard, K. *J. Physique. Lett.* **1980**, *31*, 95.

(8) Haddon, R. C. *Nature* **1975**, *256*, 394.

(9) Chi, X.; Itkis, M. E.; Reed, R. W.; Oakley, R. T.; Cordes, A. W.; Haddon, R. C. *J. Phys. Chem. B.* **2002**, *106*, 8278.

(10) Pal, S. K.; Itkis, M. E.; Tham, F. S.; Reed, R. W.; Oakley, R. T.; Haddon, R. C. *Science* **2005**, *309*, 281.

(11) Pal, S. K.; Itkis, M. E.; Tham, F. S.; Reed, R. W.; Oakley, R. T.; Donnadieu, B.; Haddon, R. C. *J. Am. Chem. Soc.* **2007**, *129*, 7163.

(12) Haddon, R. C.; Sarkar, A.; Pal, S. K.; Chi, X.; Itkis, M. E.; Tham, F. S. *J. Am. Chem. Soc.* **2008**, *130*, 13683.

(13) Pal, S. K.; Itkis, M. E.; Tham, F. S.; Reed, R. W.; Oakley, R. T.; Haddon, R. C. *J. Am. Chem. Soc*. 2008, *130*, 3942.

(14) Pal, S. K.; Bag, P.; Sarkar, A.; Chi, X.; Itkis, M. E.; Tham, F. S.; Donnadieu, B.; Haddon, R. C. *J. Am. Chem. Soc.* **2010**, *132*, 17258.
(15) Sarkar, A.; Itkis, M. E.; Tham, F. S.; Haddon, R. C. *Chem. Eur. J.* **2011**, *17*, 11576.
(16) Bag, P.; Itkis, M. E.; Pal, S. K.; Bekyarova, E.; Donnadieu, B.; Haddon, R. C. *J. Phys. Org. Chem.* **2012**, *25*, 566.
(17) Pal, S. K.; Bag, P.; Itkis, M. E.; Tham, F. S.; Haddon, R. C. *J. Am. Chem. Soc.* **2014**, *136*, 14738.
(18) Brusso, J. L.; Cvrkalj, K.; Leitch, A.; Oakley, R. T.; Reed, R. W.; Robertson, C. M. *J. Am. Chem. Soc.* **2006**, *128*, 15080.
(19) Mailman, A.; Winter, S. M.; Yu, X.; Robertson, C. M.; Yong, W.; Tse, J. S.; Secco, R. A.; Liu, X.; Dube, P. A.; Howard, J. A. K.; Oakley, R. T. *J. Am. Chem. Soc.* **2012** *134*, 9886.
(20) Yu, X.; Mailman, A.; Lekin, K.; Assoud, A.; Robertson, C. M.; Noll, B. C.; Campana, C. F.; Howard, J. A. K.; Dube, P. A.; Oakley, R. T. *J. Am. Chem. Soc.* **2012**, *134*, 2264.
(21) Leitch, A. A.; Lekin, K.; Winter, S. M.; Downie, L. E.; Tsuruda, H.; Tsell, J. S.; Mito, M.; Desgreniers, S.; Dube, P. A.; Zhang, S.; Liu, Q.; Jin, C.; Ohishi, Y.; Oakley, R. T. *J. Am. Chem. Soc*. **2011**, *133*, 6051.
(22) Wong, J. W. L.; Mailman, A.; Lekin, K.; Winter, S. M.; Yong, W.; Zhao, J.; Garimella, S. V.; Tse, J. S.; Secco, R. A.; Desgreniers, S.; Ohishi, Y.; Borondics, F.; Oakley, R. T. *J. Am. Chem. Soc*. **2014**, *136*, 1070.
(23) Ratera, I.; Veciana, J. *Chem. Soc. Rev*. **2012**, *41*, 303.
(24) Guasch, J.; Grisanti, L.; Lloveras, V.; Vidal-Gancedo, J.; Souto, M.; Morales, D. C.; Vilaseca, M.; Sissa, C.; Painelli, A.; Ratera, I.; Rovira, C.; Veciana, J. *Angew. Chem. Int. Ed*. **2012**, *51*, 11024.
(25) Guasch, J.; Grisanti, L.; Souto, M.; Lloveras, V.; Vidal-Gancedo, J.; Ratera, I.; Painelli, A.; Rovira, C.; Veciana, J. *J. Am. Chem. Soc*. **2013**, *135*, 6958.
(26) Souto, M.; Guasch, J.; Lloveras, V.; Mayorga, P.; López-Navarrete, J. T.; Casado, J.; Ratera, I.; Rovira, C.; Painelli, A.; Veciana, J. *J. Phys. Chem. Lett*. **2013**, *4*, 2721.
(27) Souto, M.; Solano, M. V.; Jensen, M.; Bendixen, D.; Delchiaro, F.; Girlando, A.; Painelli, A.; Jeppesen, J. O.; Rovira, C.; Ratera, I.; Veciana, J. *Chem. Eur. J*. **2015**, *21*, 8816.
(28) Kresse, G.; Hafner, J. *Phys. Rev. B* **1993**, *47*, 558.
(29) Kresse, G.; Furthmüller, J. *Phys. Rev. B* **1996**, *54*, 11169.
(30) Perdew, J. P.; Burke, K.; Ernzerhof, M. *Phys. Rev. Lett.* **1996**, *77*, 3865.
(31) Koepernik, K.; Eschrig, H. *Phys. Rev. B* **1999**, *59*, 1743.
(32) Kotliar, G.; Vollhardt, D. *Physics Today* **2004**, *57*, 53.
(33) Zhao, Y.; Truhlar, D. G. *Theor Chem Account* **2006**, *120*, 215.
(34) Gaussian 09, Revision A.02, M. J. Frisch, G. W. Trucks, H. B. Schlegel, G. E. Scuseria, M. A. Robb, J. R. Cheeseman, G. Scalmani, V. Barone, B. Mennucci, G. A. Petersson, H. Nakatsuji, M. Caricato, X. Li, H. P. Hratchian, A. F. Izmaylov, J. Bloino, G. Zheng, J. L. Sonnenberg, M. Hada, M. Ehara, K. Toyota, R. Fukuda, J. Hasegawa, M. Ishida, T. Nakajima, Y. Honda, O. Kitao, H. Nakai, T. Vreven, J. A. Montgomery, Jr., J. E. Peralta, F. Ogliaro, M. Bearpark, J. J. Heyd, E. Brothers, K. N. Kudin, V. N. Staroverov, R. Kobayashi, J. Normand, K. Raghavachari, A. Rendell, J. C. Burant, S. S. Iyengar, J. Tomasi, M. Cossi, N. Rega, J. M. Millam, M. Klene, J. E. Knox, J. B. Cross, V. Bakken, C. Adamo, J. Jaramillo, R. Gomperts, R. E. Stratmann, O. Yazyev, A. J. Austin, R. Cammi, C. Pomelli, J. W. Ochterski, R. L. Martin, K. Morokuma, V. G. Zakrzewski, G. A. Voth, P. Salvador, J. J. Dannenberg, S. Dapprich, A. D. Daniels, O. Farkas, J. B. Foresman, J. V. Ortiz, J. Cioslowski, and D. J. Fox, Gaussian, Inc., Wallingford CT, 2009.
(35) Rodríguez, S.; Nieto-Ortega, B.; González-Cano, R. C.; Lloveras, V.; Novoa, J. J.; Mota, F.; Vidal-Gancedo, J.; Rovira, C.; Veciana, J.; Del Corro, E.; Taravillo, M.; Baonza, V. G.; López-Navarrete, J. T.; Casado, J. *J. Chem. Phys.* 2014, *140*, 164903/1-164903/9.
(36) Hattori, Y.; Kusamoto, T.; Nishihara, H. *Angew. Chem. Int. Ed.* **2014**, *53*, 11845.
(37) Yuan, H.; Wang, K.; Yang, K.; Liu, B.; Zou, B. *J. Phys. Chem. Lett.* **2014**, *5*, 2968.
(38) Schmidtke, J. P.; Kim, J.-S.; Gierschner, J.; Silva, C.; Friend, R. H. *Phys. Rev. Lett.* **2007**, *99*, 167401.
(39) Armet, O.; Veciana, J.; Rovira, C.; Riera, J.; Castañer, J.; Molins, E.; Rius, J.; Miravitlles, C.; Olivella, S.; Brichfeus, J. *J. Phys. Chem.* **1987**, *91*, 5608.
(40) Baonza, V. G.; Taravillo, M.; Arencibia, A.; Cáceres, M.; Núñez, J. *J. Raman Spectrosc.* **2003**, *34*, 264.
(41) Del Corro, E.; González, J.; Taravillo, M.; Flahaut, E.; Baonza, V. G. *Nano Lett.* **2008**, *8*, 2215.

Pressure-induced Conductivity in a Neutral Non-Planar Spin-Localized Radical

Manuel Souto, HengBo Cui, Miriam Peñá-Álvarez, Valentín G. Baoza, Harald O. Jeschke, Milan Tomic, Roser Valentí, Davide Blasi, Imma Ratera, Concepció Rovira, and Jaume Veciana